Article

Development of a Sustainable Tungsten and Iron Bimetal-Immobilized SBA-15 Composite for Enhanced Wet Catalytic Oxidation of Dye Capacity

Taral Patel, Vishal J. Mayani, and Suranjana V. Mayani*

Read Online

ACCESS | Metrics & More | Article Recommendations

ABSTRACT: In this study, wet catalytic decomposition of Orange (II) dye was carried out with tungsten and iron bimetal-incorporated mesoporous SBA-15 (W-Fe@SBA-15) under visible light. The synthesized hybrid composite material was characterized by physicochemical methods, powder X-ray diffraction (PXRD) spectroscopy, scanning electron microscopy combined with energy-dispersive X-ray (SEM−EDX) spectroscopy studies, Fourier transform infrared (FT-IR) spectroscopy, transmission electron microscopy (TEM), atomic force microscopy (AFM), thermogravimetric analysis (TGA), and surface property studies to understand the nature of the dye degradation process and for catalytic studies. The maximum degradation of Orange (II) dye measured by a UV−visible spectrophotometer was 99% at a contaminant volume of 2.7×10^{-4} mol/L and a catalyst quantity of 2 g/L in 140 min reaction time. Using gas chromatography−mass spectrometry (GC−MS), the final products were chemically identified. The mechanistic steps of the process were carried out through a series of experiments. The recyclability of the catalyst added a novel feature for such a heterogeneous catalysis that can reduce secondary pollutants in water with no leaching effect observed.
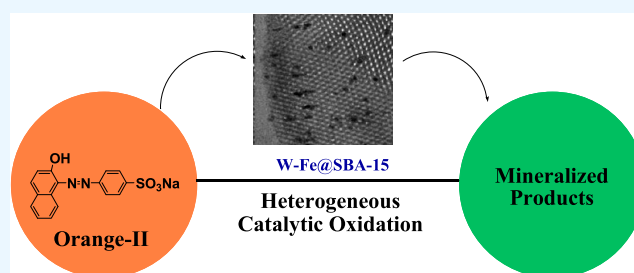
1. INTRODUCTION

Porous materials are recognized and classified on the basis of the pore size. They include mesoporous, macroporous, or microporous materials, having pore diameters in the range of 2−50 nm, higher than 50 nm, and lower than 2 nm, respectively. One of the distinctive mesoporous bases on silica is Santa Barbara Amorphous (SBA-15), which has a uniform pore size distribution and a well-organized hexagon ring framework of up to 30 nm. Mesoporous SBA-15, a material with novel structural characteristics, has been described by researchers as having a high specific surface area with active sites, consistent pore diameter for molecular diffusion and adsorption, plentiful pore walls, and excellent hydrothermal stability. These are the reasons for the wide application of such materials in industries also. SBA-15 has been considered as a good example for future scientists in material chemistry. This material has been used in a variety of fields, including catalysis, water treatment, sensor technology, and supporting cells for composite materials.[1] The current focus of research has been the growth of pore diameters into the mesopore region, which enables larger molecules to pass through the pore system. As a result, mesoporous materials have gained popularity as catalysts in industrial applications over other zeolites.[2] Physical, chemical, and biological factors predictably damage contaminants.[3] Several investigations described the incorporation of Fe, Cr, Ti, Co, Ni, and Al in the scaffold of SBA-15 by

altering the pH or employing hydrothermal synthesis methods.[4] Organofunctionalized mesoporous silica materials have been reported with improved dye sorption capacity. Previously, we have also reported that Iron-Nickel@SBA-15 can be used as a heterogeneous catalyst for the degradation of phenol-substituted molecules in water.[4] However, in this study, our focus is to incorporate tungsten−iron into mesoporous silica materials to improve their catalytic activity. Very few studies have been reported on the two-dimensional (2D) hexagonal molecular sieve SBA-15 for wet catalytic oxidation of dyes, which can be applied in wastewater treatment. Trials are being carried out by researchers to advance this hexagonal material with improved catalytic and adsorption activity using simple transition metal impregnation. Kumaravel et al.[5] combined various transition metals with mesoporous SBA-15 to increase their catalytic activity in several organocatalytic reactions such as degradation of dyes, sulfur removal, and cyclopentene oxidation with metal-supported materials, such as $WO_3@SBA-15$, W-Ti@SBA-15, $Ag@WO_3@rGO$, carbon-rich
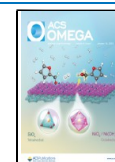
Shungite-associated ZnS-WO$_3$-CoFe$_2$O$_4$, WO$_3$/TiO$_2$, MoS$_2$-CdS/WO$_3$-MnO$_2$, Gd@WO$_3$NRs, Cd$_{0.85}$Zn$_{0.15}$S@WO$_3$/WS$_2$, and WO$_3$/MoS$_2$.[5] Recently, Zn$_{0.9}$ M$_{0.06-x}$ Li$_x$O (M: Al^{3+}, Cr^{3+}, Fe^{3+}) nanocomposites with aliovalent cation substitutions were characterized by Ansari et al.[6] as having exceptionally strong photocatalytic capabilities toward the degradation of rhodamine B. The outcomes revealed that after 3 h of UV illumination, Eu$_2$O$_3$ and zinc oxide (ZnO) nanoparticles showed the greatest photocatalytic activity of 96.5% with methylene blue dye.[7]

For the removal of organics, several processes can be applied, but they depend on the reusability and efficiency of the catalyst. Thermal treatments release significant amounts of harmful materials; microorganisms typically require a long time to degrade pollutants due to the toxicity of the product. Advanced oxidation procedures, which have been described as appropriate for a nearly ambient breakdown of miscible organic pollutants from soil as well as water and achieve practically 100% degradation, are alternatives to these well-established strategies.[3] Water and soil environments are contaminated due to increasing industrial development and the high rate of population increase. Environmental pollution is mainly caused by organics such as dyes, agrochemicals, and pharmaceuticals. Among these, organic dyes are highly toxic molecules and are used frequently in the textile and leather industries. In large fine chemical, polymeric plastic, and food industries, hazardous dye pigments are commonly used and discharged into the surroundings.[5] Synthetic dyes known as azo-dyes are difficult to break down, and the breakdown byproducts are exceedingly poisonous and carcinogenic. Dye-based products from the textile industry are dangerous sources of environmental pollution.[8] These include compounds with one or more azo linkages as chromophore groups ($-N{=}N-$) in combination with aromatic structures that have functional groups such as $-OH$ and $-SO_3H$,[9] including some of the most toxic and carcinogenic synthetic colors.

In this framework, the present study aims to develop a novel, simple, and environmentally friendly process for bimetallic **W-Fe@SBA-15** composite synthesis through a hydrothermal in situ method. Orange (II) dye has been chosen as the contaminant in our study. Orange (II) dye in waste discharges is stable and difficult to degrade under ecological conditions. Therefore, the catalytic wet oxidation of Orange (II) dye has been adopted as an advanced, cheap, and powerful technique using the newly synthesized **W-Fe@SBA-15** catalyst and hydrogen peroxide, which can be combined with an environmentally friendly, nonspecific oxidant that is acceptable for degrading contaminants to create OH radicals.

2. MATERIALS AND METHOD

2.1. Materials.
The pluronic triblock copolymer PEG-PPG-PEG (P123; Aldrich), aqueous solution of hydrogen chloride (HCl; Molychem, India), tetraethoxy silane (Aldrich), iron(III) nitrate nonahydrate (Sisco Research Laboratories, Mumbai, India), and sodium tungstate dihydrate (Aldrich) were purchased. The reactions were conducted with Orange (II) dye (Alfa Aesa, U.K.), H$_2$O$_2$ (Loba Chemie, India) and the stock solution of the reactant at 2.7 × 10^{-4} mol/L in distilled water.

2.2. Material Preparation Process.
For advancement of application, a new process of composite synthesis was carried out. SBA-15 was synthesized using the hydrothermal crystallization process. First, 4.0 g of P123 was dissolved in

30 g of double-distilled water and agitated for 3 h. Then, 120 g of 2 N HCl was added to the resulting solution while being agitated, and 9.5 mL of TEOS was added dropwise as a source of silica. The mixture was stirred constantly at 313 K for 24 h, then put into an autoclave lined with Teflon and held there for 48 h. The product underwent filtering, washing, and air drying at 383 K. The acquired sample was calcined in air for 6 h at 823 K; the yield was 6.3 g. Fe(NO$_3$)$_3$·9H$_2$O as iron and Na$_2$WO$_4$·2H$_2$O as tungsten precursors were used to prepare **W-Fe@SBA-15**. Fe(NO$_3$)$_3$·9H$_2$O (1 g), Na$_2$WO$_4$·2H$_2$O (1 g), and SBA-15 (2 g) were combined in 30 mL of deionized water and stirred for 1 h as part of the wet impregnation procedure. **W-Fe@SBA-15** was produced from the combination after it had been dried at 353 K and calcined in air for 3 h at 823 K; yield: 3.9 g. The dried material was thoroughly crushed with a mesh size of 400 (0.037 mm). FT-IR (KBr) v- 483, 798, 988, 1086, 1835, 2031, and 3449 cm^{-1}. ICP analysis of the **W-Fe@SBA-15** catalyst revealed 6.06 wt % iron and 10.77 wt % tungsten metal.

2.3. Characterization.
X-ray diffraction in powder form (Phillips, the Netherland) throughout the two ranges was used to analyze the hybrid composite material. FT-IR spectroscopy (Perkin-Elmer Spectrometer) was performed utilizing KBr pellets. A metal detection technique (inductively coupled plasma optical emission spectroscopy, ICP-OES) was used to categorize SBA-15-incorporated metals (JY Ultima 2CHR). Surface area analysis was accomplished with nitrogen adsorption−desorption data acquired at 77 K using a volumetric adsorption setup (Micromeritics ASAP-2010). The pore size of the composite material was calculated using the Barrett−Joyner−Halenda (BJH) model and the nitrogen adsorption−desorption isotherm. The thermal behavior and microstructure of the metal composite were analyzed by thermogravimetric analysis (TGA, TA instrument) in the temperature range of 30−800 °C (heating rate 10 °C/min) in an air atmosphere with a flow rate of 60 cm^3/min. With the aid of high-resolution scanning electron microscopy coupled with energy-dispersive X-ray (SEM−EDX, LEO-1430, U.K.), transmission electron microscopy (TEM, Jeol Corporation, Japan), and atomic force microscopy (AFM, NT-MDT, Ntegra Aura, the Netherlands) analyses, the surface morphology, elemental identification, and quantitative compositional information of the material were ascertained. The ingredients were finely ground and blended with ethanol. The suspension of the substance was dripped over a carbon grid and allowed to dry naturally. AFM measurements were performed using samples connected to a mica plate that had been coated with polylysine in both contact and semi-contact modes.

2.4. Catalytic Wet oxidation of Orange (II).
Orange (II) dye was catalytically degraded in a round-bottom flask (RBF) and condenser glass assembly. Using 2 g/L **W-Fe@SBA-15** catalyst, the oxidation reaction of 50 mL of Orange (II) dye (2.7 × 10^{-4} mol/L) and 50 mL of H$_2$O$_2$ (10^{-4} mol/L) was performed for 140 min at 30 °C (room temperature), ambient pressure, and 180 rpm. The centrifugation method was used to isolate the catalyst, **W-Fe@SBA-15**, once the reaction was finished. Using UV−visible spectroscopy, the complete deterioration of Orange (II) dye was observed (Varian, Cary-4000, wavelength 486 nm). Gas chromatography-coupled mass spectroscopy (GC−MS) was used for the identification of products. Following the catalytic run, the final products were extracted using equal amounts of chloroform and the product aqueous mixture. Two different layers of the mixture were
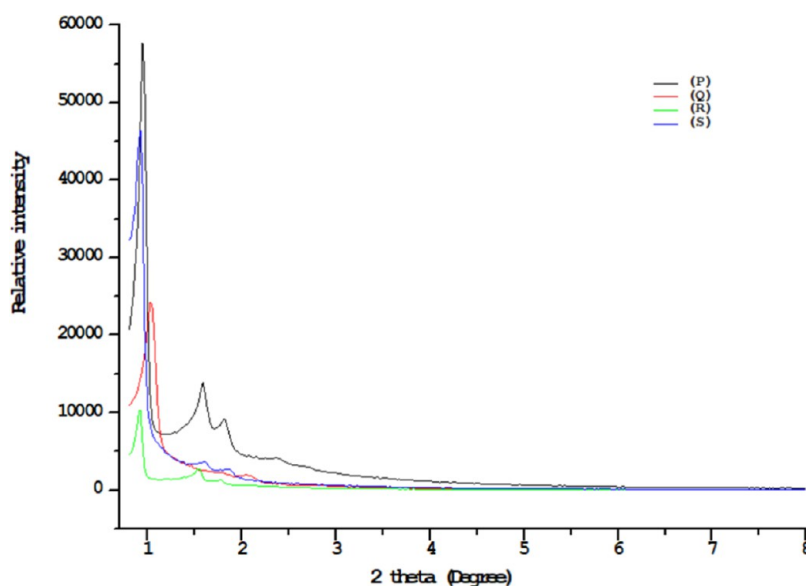
Figure 1. Low-angle powder XRD of SBA-15 (P), Fe@SBA 15 (Q), W@SBA-15 (R), and **W-Fe@SBA-15** (S).
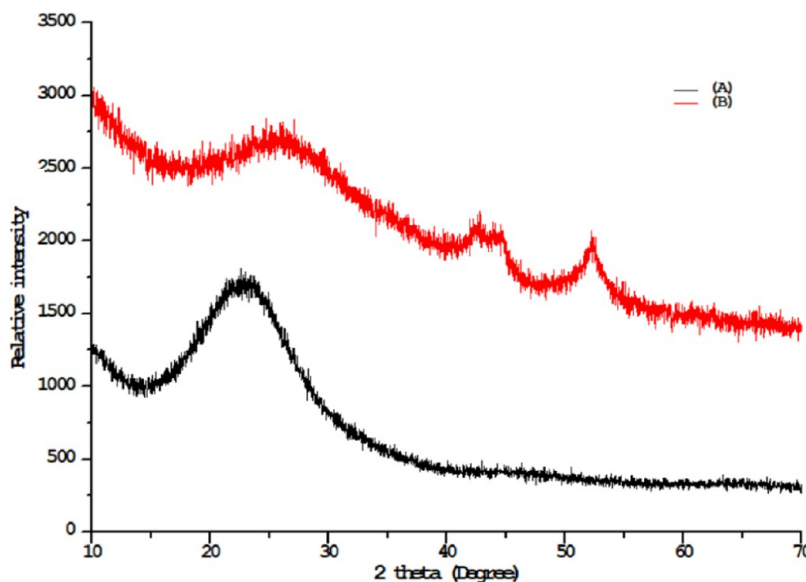

Figure 2. High-angle powder XRD of SBA-15 (A) and **W-Fe@SBA-15** (B).

allowed to settle after being sonicated for 10 min. The gas chromatography-coupled mass spectroscopy (GC−MS) study was executed using 0.6 μL of the extracted chloroform sample layer (Shimadzu). The injection temperature of GC−MS was 250 °C. The preliminary temperature was controlled at 50 °C for 5 min before being increased to 180 °C at a rate of 10 °C/min. This temperature was maintained for more than 5 min, again increased to 250 °C at a rate of 10 °C/min, and then again maintained for 5 min.

3. RESULTS AND DISCUSSION

3.1. Physicochemical Characterization. *3.1.1. Powder X-ray Diffraction (PXRD) Analysis.* Powder X-ray diffraction was employed for the complete assessment of the crystalline structure and morphology of the prepared composite material. In low-angle PXRD patterns, SBA-15 samples are well resolved and show three characteristic peaks at 2θ = 0.94, 1.60, and 1.82°. The main sharp peak recognized from the hexagonal

lattice structure is attributed to the Bragg reflection from the (100) plane along with small peaks with low strength equivalent to the (110) and (200) reflection planes. After the immobilization of SBA-15 with W−Fe bimetals, the strength of all of the peaks declined slightly with a minor shift of 2θ values. Figure 1 indicates that the structure has not been disrupted due to the modification of SBA-15. The values for **W-Fe@SBA-15** were found to be 0.96, 1.59, and 1.86°, which might be possible due to the metal present inside the pores. This leads to a higher scattering of powder inside the pores, which causes a loss of peak strength considering the phase withdrawal between the metal and pore walls.[10,11] The peak positions with a slight change in the 2θ values were determined using PXRD patterns of SBA-15, Fe-, W-, and Fe-W in addition to SBA-15 (Figure 1). XRD peaks were observed at 2θ = 1.01, 1.42, and 1.79° for Fe@SBA-15 and 0.95, 1.58, and 1.75° W@SBA-15.
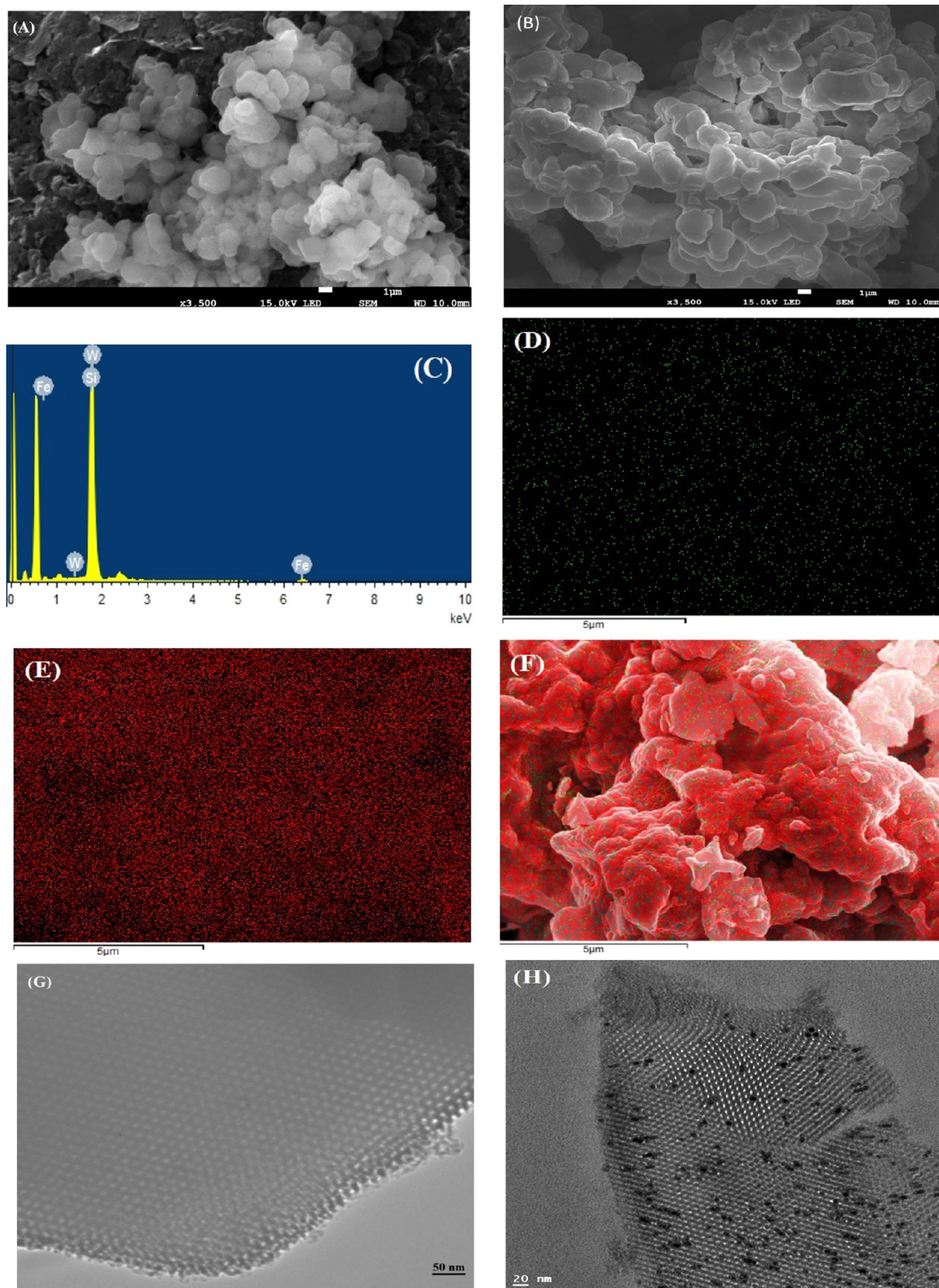
Figure 3. SEM images of SBA-15 (A) and **W-Fe@SBA-15** (B). EDX mapping of **W-Fe@SBA-15** (C). Distribution of **Fe**, **W**, and SBA-15 (D−F). TEM images of SBA-15 (G) and **W-Fe@SBA-15** (H).

Even after impregnation, the broad-angle X-ray pattern reveals the presence of primary reflections comparable to those of SBA-15, indicating the characteristic nature of the

mesoporous SBA-15 framework (Figure 2). A wide peak pattern at $2\theta = 23.30°$ is assigned to silicone dioxide (a component of SBA-15).[4] For the metal-supported catalyst,
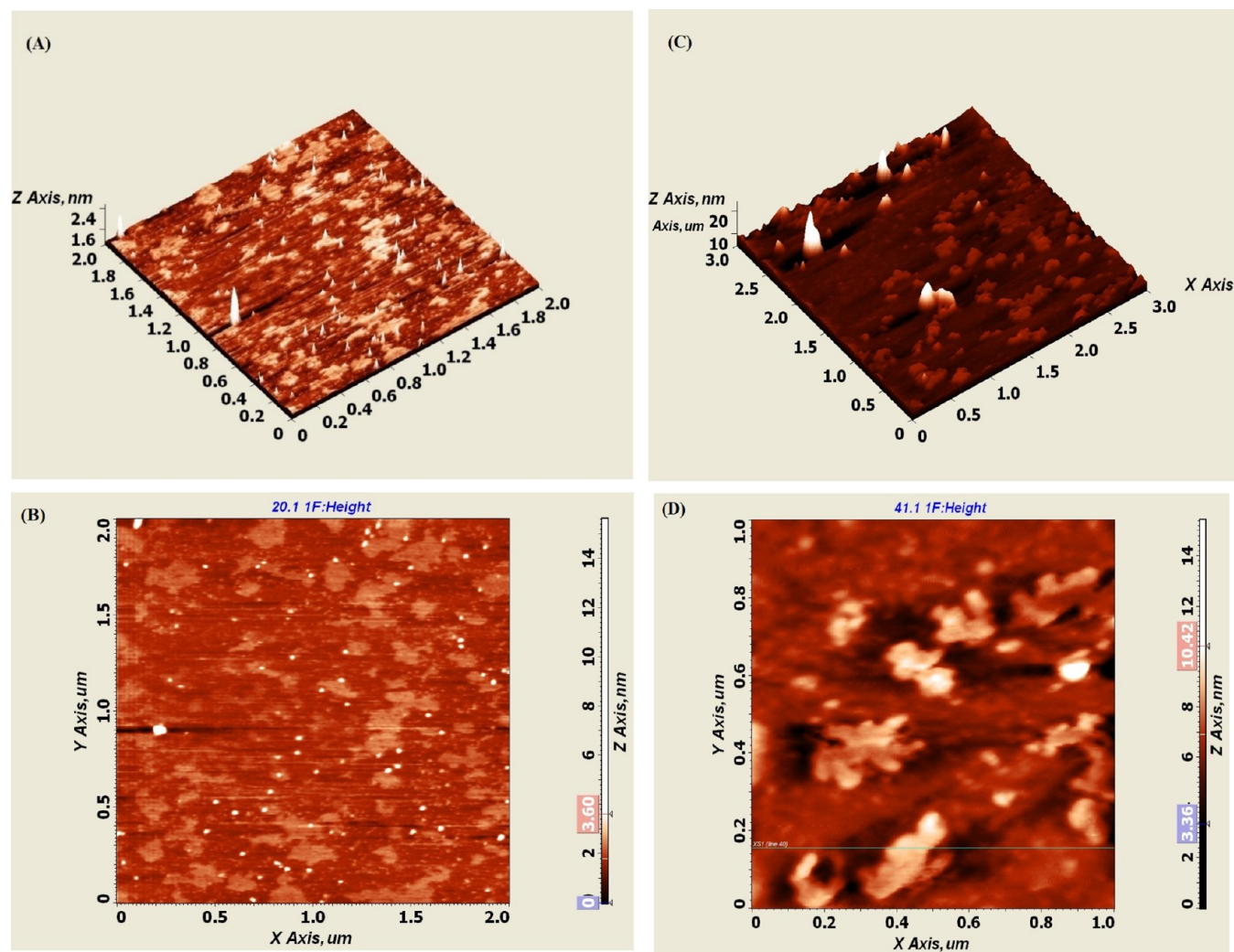
Figure 4. AFM images of the surface of SBA-15 silica film (A, B) and W−Fe-immobilized SBA-15 (C, D).

high-angle XRD peaks at 2θ = 20.45, 42.62, 44.44, and 52.23° (**W-Fe@SBA-15**) were seen.[10] Despite the presence of iron in **W-Fe@SBA-15**, no similarities to Fe_2O_3 on the mesoporous crystalline silica surface as expressed in high-angle XRD were detected (range 10−80). A highly ordered SBA-15 structure was reserved in the metal-incorporated SBA-15 composite. On mesoporous silica, there were no apparent Fe_2O_3 diffraction peaks in the wide-angle range XRD of the catalyst. The surface of SBA-15 showed an even distribution of iron species.[4] The metals were distributed well inside the pores of SBA-15. The excellent match suggested the similarity in their crystalline nature.

3.1.2. Microscopic Characterization [Scanning Electron Microscopy−Energy-Dispersive X-ray (SEM−EDX), Transmission Electron Microscopy (TEM), and Atomic Force Microscopy (AFM) Analyses]. The SBA-15 (Figure 3A) samples had tiny agglomerates, as seen in SEM micrographs. After metal immobilization, the morphology was preserved to form **W-Fe@SBA-15** (Figure 3B). The catalysts showed mesoporous particles of a homogeneous size and an organized hexagonal shape.[10] This image showed a network of parallel channels in the composite. The elementary composition across a particle is also shown in Figure 3C. The EDX analysis showed the peaks of tungsten (W) and iron (Fe), which confirmed the immobilization of these metals on the silica

SBA-15 material (Figure 3C). The EDS mapping images showing the metal distribution of Fe, W, and SBA-15, as shown in Figure 3D−F. The metals are distributed uniformly by impregnation on SBA-15.

TEM micrographs confirmed the textural properties of SBA-15, which possessed lateral border lines in the lattice when observed from the side view, and a hexagonal porous structure was also detected through the facet of the pores (Figure 3G). SBA-15 showed mesopores of one-dimensional channels during its production in the acidic medium, indicating that it has a 2D p6mm uniform hexagon framework. Lateral border fringes confirmed the nature of border layer separation and the typically well-packed arrangement of monolayers. As demonstrated in **W-Fe@SBA-15**, the combination of the metals had no effect on the highly ordered morphology of SBA-15 (Figure 3H). As a result of the metals on SBA-15, the black aggregates were well decorated.[11]

AFM images show composites with differences in their surface morphology. The samples show good structural gathering. The clusters can be seen to have an ordered arrangement. An already tubular hexagonal characteristic structure is seen in TEM images. The irregular surface can be seen in **W-Fe@SBA-15** (Figure 4C,D) compared with SBA-15 (Figure 4A,B). The surface roughness confirmed the presence of fixed metal units on the surface. AFM was found to
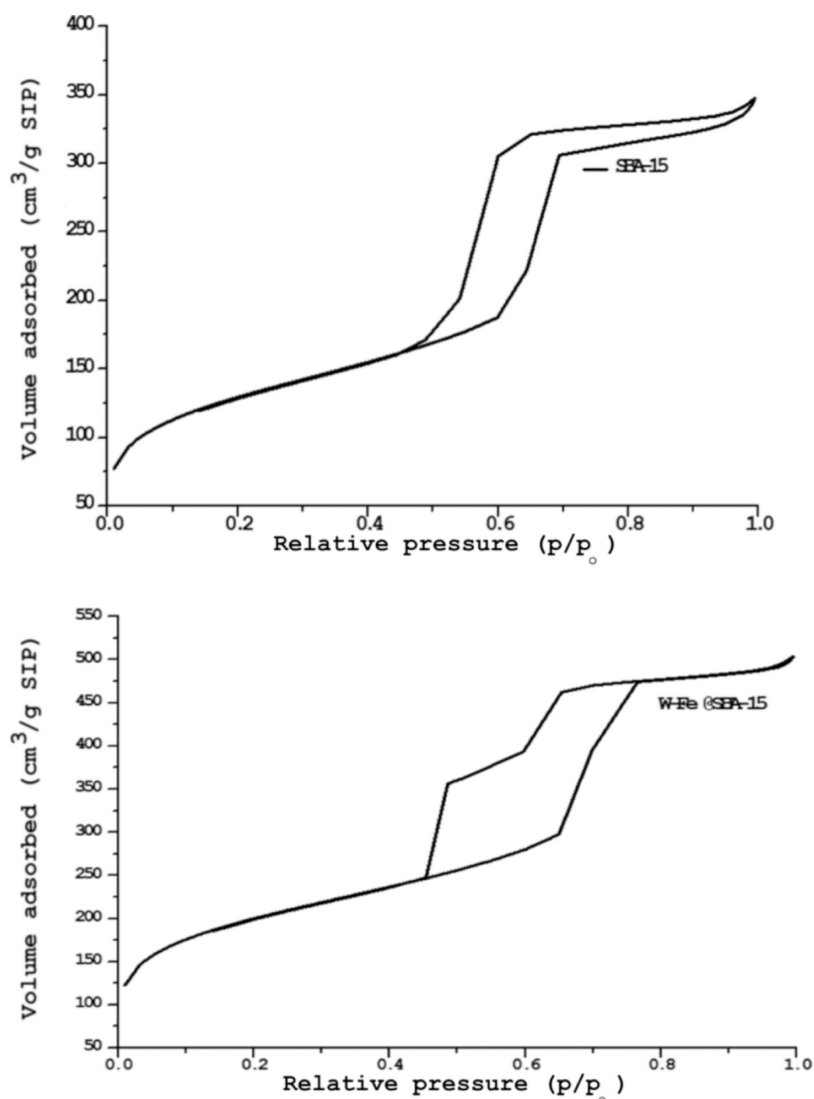
Figure 5. N_2 adsorption/desorption isotherms of SBA-15 and **W-Fe@SBA-15**.

be a useful process to study the structural topographies of the samples.[12−14] Additional comprehensive evidence was obtained by AFM observation. The AFM results confirmed that we obtained even, well-structured mesoporous films of hexagonal channels.

3.1.3. Nitrogen Adsorption−Desorption Isotherm Study. SBA-15-associated **W-Fe@SBA-15** exhibits type IV nitrogen adsorption−desorption isotherms (Figure 5), which demonstrate the presence of an ordered structure in SBA-15.[4] Table 1 provides an overview of the textural qualities, including data on the surface and pore parameters. Following the functionalization of **W** and **Fe** metals on SBA-15, the BET surface area reduced to 725 from 790 m^2/g. Similarly, a decrease in the volume and diameter of mesoporous pores to 0.759 cm^3/g and 41.7 A^0, respectively, was observed (Table 1).

Table 1. Surface and Pore Characteristics of SBA-15 and W-Fe@SBA-15

compound	BET surface area (m^2/g)	total pore volume (cm^3/g)	BJH pore diameter (Å)
SBA-15	790	1.283	78.0
W-Fe@SBA-15	725	0.759	41.7

3.1.4. Thermogravimetric Analysis (TGA). TGA results for SBA-15 and **W-Fe@SBA-15** in the temperature range of 21−800 °C showed minute weight losses of about 3.7 and 6.3%, respectively. The discharge of water is mostly responsible for this weight reduction. As a result of carbonization, SBA-15 and **W-Fe@SBA-15** consistently lose weight between 28 and 900 °C (Figure 6).

3.2. Catalytic Oxidation of Orange (II). *3.2.1. Blank Experiments.* Blank experiments were performed before examining the catalytic efficiency for the oxidative catalysis of Orange (II) under the following reaction conditions: (i) Orange (II) dye without catalyst and oxidant; (ii) equal 1:1 molar ratio of Orange (II) dye and H_2O_2 without catalyst; (iii) Orange (II) dye with SBA-15 (2 g/L); and (iv) Orange (II) dye and H_2O_2 (1:1 molar ratio) with 2 g/L SBA-15. A degradation reaction was carried out for 120 min at 298 K, atmospheric pressure, and under 200 rpm stirring with Orange (II) dye (2.7×10^{-4} mole/L) and H_2O_2 (10^{-4} mole/L). The blank experiment yielded no significant conversion.

3.2.2. Effect of the Reaction Time. Figure 7 illustrates how Orange (II) dye degradation is enhanced when the reaction time is increased from 5 to 140 min. The increase in conversion has been studied with Orange (II) (2.7×10^{-4}
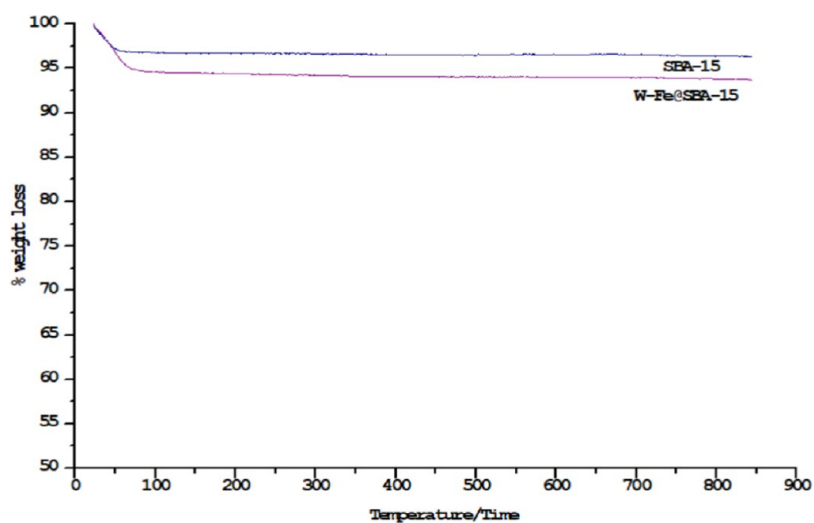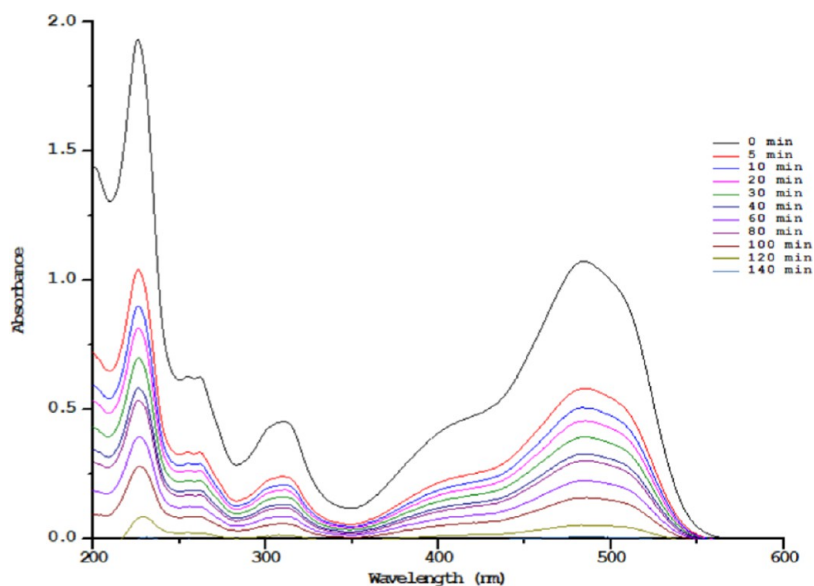
Figure 6. TGA curves of SBA-15 and **W-Fe@SBA-15**.

Figure 7. Time-dependant UV−visible spectra of Orange (II) dye solutions with **W-Fe@SBA-15**. Reaction conditions: Orange (II) dye 2.7×10^{-4} mol/L, load 2 g/L, temperature 298 K.

mol/L) and H_2O_2 (10^{-4} mol/L) at 298 K using **W-Fe@SBA-15** as the catalyst (2 g/L). Wet impregnation may have deposited a part of the metals W(II) and Fe(III) upon reachable active sites of SBA-15, which are available for the decomposition of reactants. The catalyst was found to be an excellent catalyst. After 140 min, the absorbance peak had completely vanished. This indicates that all of the components of Orange (II) dye were broken down. According to the report of the experiment by Ni et al., $ZnMn_2O_4$ was used as a photocatalyst to degrade Orange by 90%.[15] In our study, GC−MS analysis was also used to track the end products of degradation of Orange (II) dye (Scheme 1). Individual metal efficacies of Fe@SBA-15 and W@SBA-15 catalysts were found to be less than that of the bimetallic **W-Fe@SBA-15** catalyst. Figure 8 illustrates how the breakdown of the Orange (II) dye improved as the reaction time increased from 0 to 180 min. With Fe@SBA-15, W@SBA-15, and **W-Fe@SBA-15**, rapid increases in conversion from 15.1 to 64.4%, 10.2 to 70.0%, and 46.5 to 99.0%, respectively, were observed for the reactions

performed over this time frame under ideal reaction conditions.

3.2.3. Effect of pH on the Leaching Experiment. It is also crucial to determine the role of the transition metal ions (W^{2+}, Fe^{3+}) in the catalyst **W-Fe@SBA-15** in causing secondary pollution after a catalytic run. The catalysts (0.1 g) were mixed with 50 mL of water at various pH values (3.0, 4.0, 5.0, 6.0, 7.0, 8.0, and 9.0) at 298 K (standard reaction temperature) for 120 min. Removal of the attached metal from the solid catalysts was investigated. The mixture was centrifuged to determine the concentrations of **W** and **Fe** in the aqueous layer; 0.25−0.99% (**Fe**) and 0.01−0.12% (**W**) of the catalyst **W-Fe@SBA-15** were released, respectively. Although the leaching is significantly influenced by the standard pH, extensive release occurred in a basic medium. Generally, metal release is minimal and has no effect on the percentage of metals in water, which is lower than the allowable limits of drinking water measures. As per our leachability study, the quantity of metals **W** and **Fe** drained into the water is much less than the amount

Scheme 1. Schematic Degradation Pathway of Orange (II) Dye (Reaction Conditions: Orange (II) Dye 2.7 × 10⁻⁴ mol/L, Load 2 g/L, Temperature 298 K)
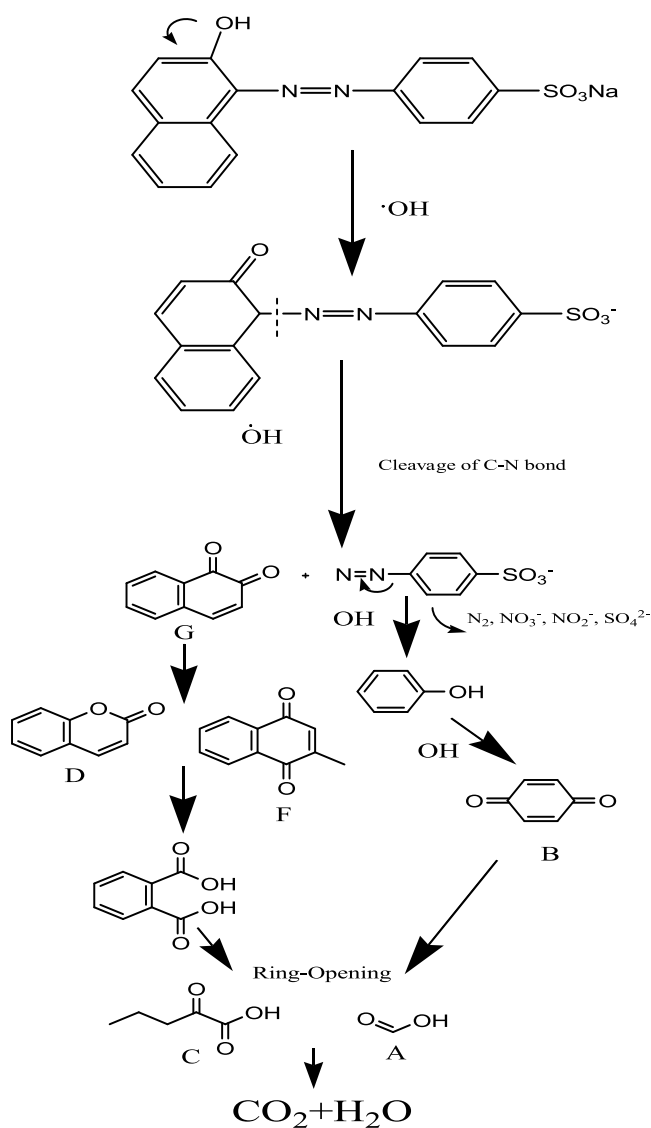
mentioned by the World Health Organization.[16] The values of iron and tungsten in natural freshwater are 0.3 and 0.003 mg/L, respectively. Therefore, our catalyst is rigid and non-problematic with regard to water pollution.

3.2.4. Effect of Temperature. Independent thermal studies were conducted to study the impact of increasing temperature on Orange (II) dye degradation, even though the majority of the experiments in the present study were conducted at 298 K or close to room temperature. The degradation increased very slightly while the reaction was continually monitored at 288, 298, 303, 308, and 313 K (Table 2). The better diffusional

Table 2. Effects of the Reaction Temperature on the Catalytic Oxidation of Orange (II) with W-Fe@SBA-15 (Load 2 g/L; Orange (II): 5 × 10⁻⁴ mol/L)

temperature (K)	W-Fe@SBA-15
288	98.1
298	99.0
303	99.2
308	99.4
313	99.4

transport of Orange (II) dye molecules from the bulk phase to the liquid−catalyst interface as well as their improved movement at higher temperatures are clearly responsible for the increase in the degrading efficiency of the catalysts. The catalytic oxidative degradation of Orange (II) dye with the catalyst, **W-Fe@SBA-15**, was improved from 98.1 (288 K) to 99.4% (313 K) at two different temperatures, respectively.[17]

3.2.5. Product Analysis. The reaction products from the **W-Fe@SBA-15** wet-catalyzed oxidation of Orange (II) dye were identified by gas chromatography−mass spectroscopy studies (Scheme 1). The catalytic reaction mechanism is based on free •OH radicals. The breakdown of both hydrogen peroxide and water molecules generates free •OH radicals and oxides during the catalytic process. It is assumed that the dissolved oxygen contributes to the generation of •OH radicals because it causes oxidation to drastically decrease with temperature.[18] Based on the products found, it is anticipated that the oxidative action of hydroxyl radicals on the C−N bond causes cleavage, which results in 4-diazenylbenzosulfonate and 1,2-naphthoquinone
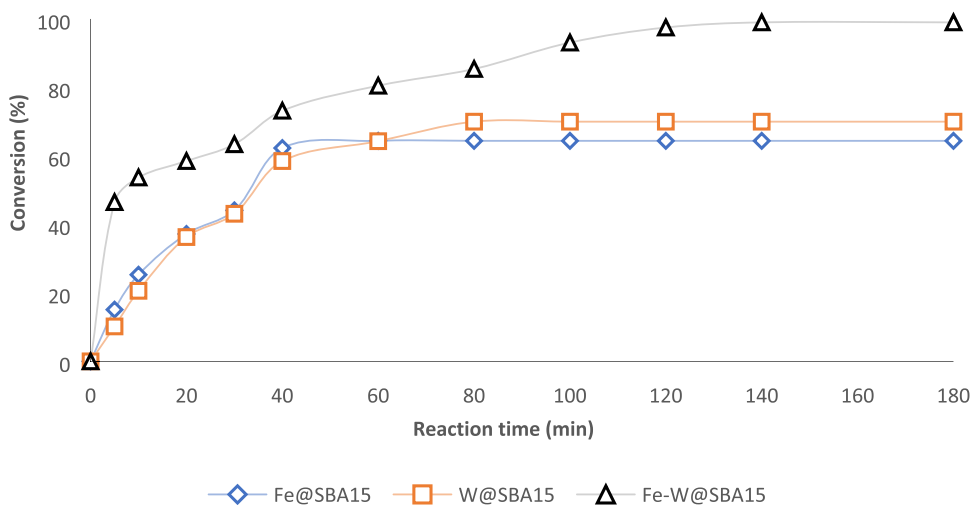
Figure 8. Effect of the reaction time with Fe@SBA-15, W@SBA-15, and **W-Fe@SBA-15** (reaction conditions: Orange (II) 2.7 × 10⁻⁴ mol/L, H_2O_2 (10⁻⁴ mole/L), load 2 g/L, temperature 298 K).
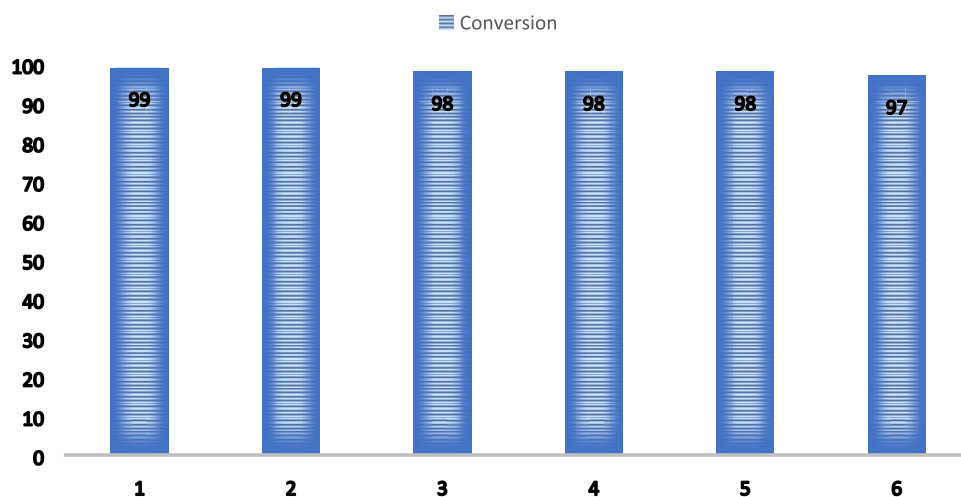
RECYCLABILITY

Figure 9. Recyclability of the catalyst (Orange (II): 2.7×10^{-4} mol/L; H_2O_2: 10^{-4} mol/L; **W-Fe@SBA-15**: 2 g/L; 60 °C, normal pressure, and 180 rpm rate).

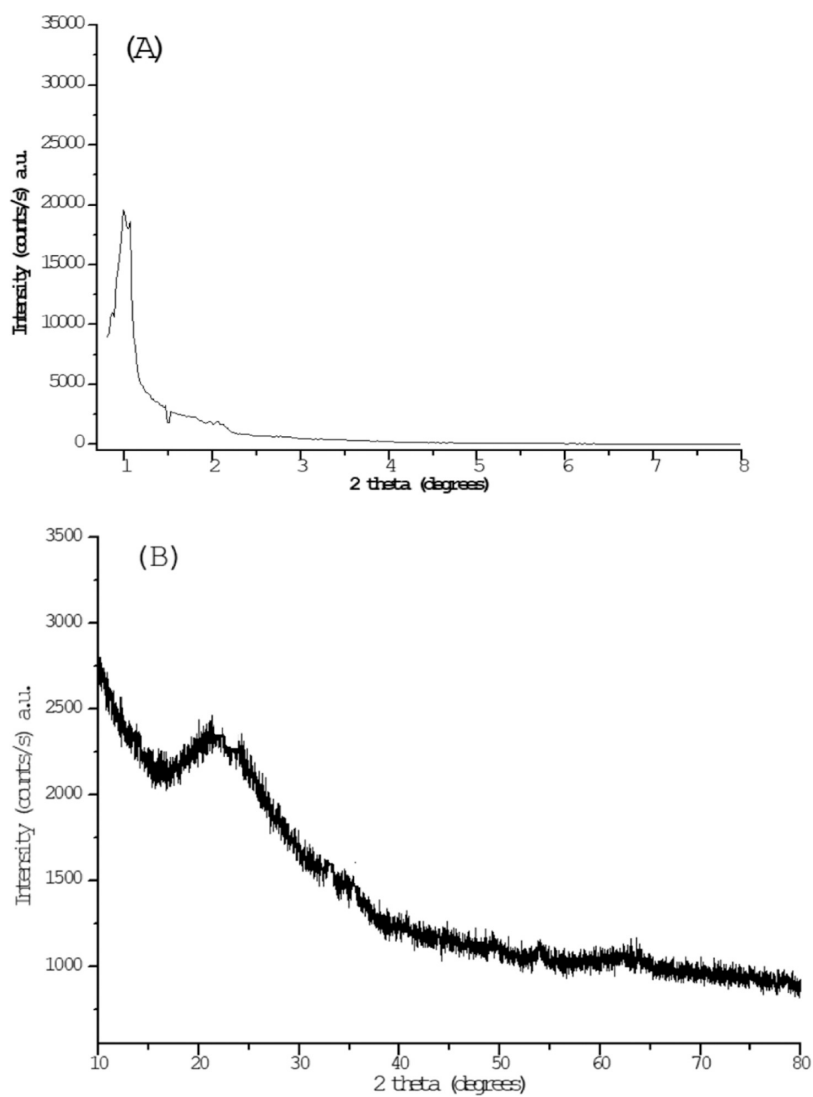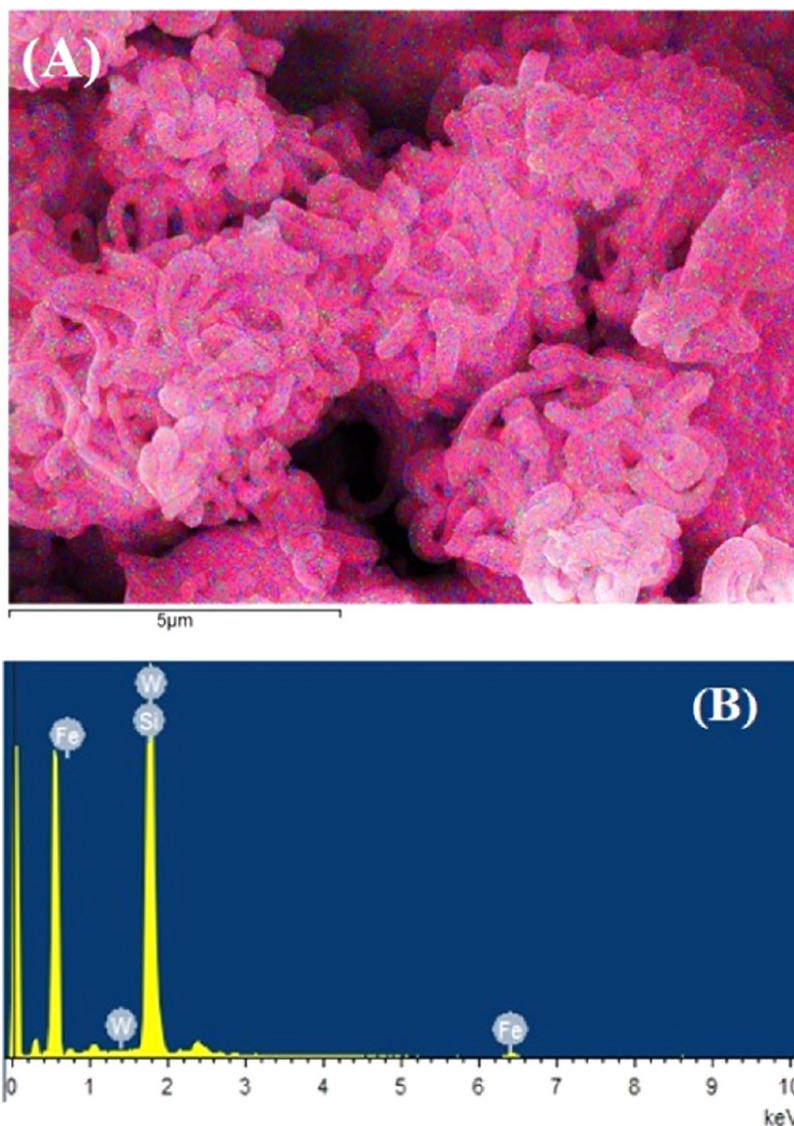**Figure 10.** Low-angle (A) and high-angle PXRD (B) of recycled **W-Fe@SBA-15**.

Figure 11. SEM images of the distribution of **Fe**, **W**, and SBA-15 (A) and EDX mapping of **W-Fe@SBA-15** (B) for recycled **Fe-W@SBA15**.

(G). It is possible that the intermediates coumarin (D) and nenadione (F) are downstream byproducts of G. They undergo additional oxidation, which causes the naphthoquinone ring to break, producing phthalic acid (E), before forming ring-opening products. 4-Diazenylbenzosulfonate is unstable and is attacked by hydroxyl radicals, which causes it to oxidize to phenol. Nitrogen from the azo group of Orange II is also used to form nitrite, nitrate, and N_2. Phenol oxidation results in the formation of benzoquinone (B), which then proceeds through ring-opening reactions to produce short-chain aliphatic acids A and C. These organic materials are finally mineralized into CO_2 and water.

3.2.6. Recyclability of the Catalysts. After completion of the catalytic run, the catalyst **W-Fe@SBA-15** was recovered from the mixture through filtration. The impure solid catalyst was cleaned and purified using the Soxhlet washing method with ethanol and water. The catalyst was completely dried and made moisture-free in a vacuum desiccator for 12 h for subsequent catalytic reactions. With the same catalyst, six catalytic runs were successfully completed without any discernible performance degradation (Figure 9). The catalyst was found to be recyclable up to six times with retention of its affordable interest under the improved response conditions. The PXRD (Figure 10) and SEM−EDS figures (Figure 11A,B) confirm the presence of **W** and **Fe** inside SBA-15, even after recycling.

4. CONCLUSIONS

We have revealed that iron and tungsten can be successfully immobilized on SBA-15 for **W-Fe@SBA-15**. SBA-15 is catalytically inactive by itself, but when transition metals are added, the substance can be transformed into a well-organized catalyst for the treatment of water contaminated by Orange (II). The catalytic elimination of Orange (II) by metal-incorporated SBA-15 is regarded as an active technique in accordance with the postulated breakdown pathway and the intermediates. The degradation products were not long-lasting contaminants. The products 2,4-hexadienedioic acid, isopropanol, and acetic acid were identified by GC−MS analyses. Another benefit of the decomposition method was the recyclability of the catalyst. Iron and nickel metals did not cause any water contamination issues, according to the leaching experiment.

AUTHOR INFORMATION

Corresponding Author

Suranjana V. Mayani − *Department of Chemistry, Marwadi University, Rajkot 360003 Gujarat, India;* ⓞ orcid.org/0000-0002-2624-3305; Email: suranjana.mayani@marwadieducation.edu.in

Authors

Taral Patel − *Department of Physical Chemistry and Technology of Polymers, Faculty of Chemistry, Silesian University of Technology, Gliwice 44-100, Poland*

Vishal J. Mayani − *Hansgold ChemDiscovery Center (HCC), Hansgold ChemDiscoveries Pvt. Ltd., Rajkot 360004 Gujarat, India*

Complete contact information is available at:
https://pubs.acs.org/10.1021/acsomega.2c04549

Author Contributions

S.V.M.: resources, design of the project, supervision, writing of the manuscript and editing. T.P.: methodology, catalyst synthesis and characterization, writing. V.J.M.: Investigation of catalytic reaction, catalyst optimization and recycling activity, degradation product identification, writing of the original draft.

Notes

The authors declare no competing financial interest.

All data analyzed during this study are included in this published article.

REFERENCES

(1) Thahir, R.; Abdul Wahid, W.; Nursiah La, N.; Indah, R. Synthesis of High Surface Area Mesoporous Silica SBA-15 by Adjusting Hydrothermal Treatment Time and the Amount of Polyvinyl Alcohol. *Open Chem.* 2019, 17, 963−971.

(2) Chaudhary, V.; Sweta, S. An Overview of Ordered Mesoporous Material SBA-15: Synthesis, Functionalization and Application in Oxidation Reactions. *J. Porous Mater.* 2017, 24, 741−749.

(3) Mayani, S. V.; Mayani, V. J.; Sang, W. K. Catalytic Oxidation of Phenol Analogues in Aqueous Medium over Fe/SBA-15. *Bull. Korean Chem. Soc.* 2012, 33, 3009−3016.

(4) Mayani, S. V.; Mayani, V. J.; Kim, S. W. SBA-15 Supported Fe, Ni, Fe-Ni Bimetallic Catalysts for Wet Oxidation of Bisphenol-A. *Bull. Korean Chem. Soc.* 2014, 35, 3535−3541.

(5) Kumaravel, S.; Thiripuranthagan, S.; Vembuli, T.; Erusappan, E.; Durai, M.; Sureshkumar, T.; Durai, M. Fabrication of Mesoporous WO3-SBA-15 Catalysts and Enhanced Photocatalytic Degradation of Harmful Dyes. *Optik.* 2021, 235, 166599.

(6) Ansari, S. A.; Manjunatha, C.; Parveen, N.; Shivaraj, B. W.; Hari krishna, R. Mechanistic insights into defect chemistry and tailored photoluminescence and photocatalytic properties of aliovalent cation substituted $Zn_{0.94}M_{0.06−x}Li_xO$ (M: Fe3+, Al3+, Cr3+) nanoparticles. *Dalton Trans.* 2021, 50, 14891−14907.

(7) Mohamed, W. S.; Abu-Dief, A. M. Synthesis, characterization and photocatalysis enhancement of Eu_2O_3-ZnO mixed oxide nanoparticles. *J. Phys. Chem. Solids* 2018, 116, 375−385.

(8) El-Khalafy, S. H.; Hassanein, M. T.; Abd-Elal, M. F.; Atia, A. A. Oxidation of Azo Dye Orange II with Hydrogen Peroxide Catalyzed by 5,10,15,20-Tetrakis[4-(Diethylmethylammonio)Phenyl]-Porphyrinato-Cobalt(II)Tetraiodide in Aqueous Solution. *J. Saudi Chem. Soc.* 2020, 24, 520−526.

(9) García, E.; Ricardo, L. M.; Marcos, M. L.; Isaías, H. P.; Maria, J. V.; Franco, A. M. M. Adsorption of Azo-Dye Orange II from Aqueous Solutions Using a Metal-Organic Framework Material: Iron-Benzenetricarboxylate. *Materials* 2014, 7, 8037−8057.

(10) Ruchomski, L.; Stanisław, P.; Tomasz, P.; Edward, M.; Marek, K. Synthesis and Properties of Fe/SBA-15. *Colloids Surf., A* 2020, 599, No. 124922.

(11) Chang, F.; Jie, W.; Jieru, L.; Junrong, S.; Baoqing, D.; Hu, X. Enhanced Visible-Light-Driven Photocatalytic Performance of Mesoporous W-Ti-SBA-15 Prepared through a Facile Hydrothermal Route. *Colloids Surf., A* 2016, 499, 69−78.

(12) Zauska, L.; Stefan, B.; Eva, B.; Jozef, B.; Matej, B.; Vladimir, Z.; Virginie, H.; Miroslav, A. Thermosensitive Drug Delivery System SBA-15-PEI for Controlled Release of Nonsteroidal Anti-Inflammatory Drug Diclofenac Sodium Salt: A Comparative Study. *Materials* 2021, 14, 1−25.

(13) Barczak, M.; Oszust, M.; Michalak, K.; Gdula, K.; Pasieczna-Patkowska, S.; Zięba, E.; Dąbrowski, A. Functionalized SBA-15 Organosilicas as Sorbents of Mercury(II), Cadmium(II) and Copper-(II). *Glass Phys. Chem.* 2014, 40, 41−48.

(14) Laskowski, L.; Laskowska, M.; Jelonkiewicz, J.; Dulski, M.; Wojtyniak, M.; Fitta, M.; Balanda, M. SBA-15 Mesoporous Silica Free-Standing Thin Films Containing Copper Ions Bounded via Propyl Phosphonate Units-Preparation and Characterization. *J. Solid State Chem.* 2016, 241, 143−151.

(15) Ni, Q.; Cheng, H.; Ma, J.; Kong, Y.; Komarneni, S. Efficient Degradation of Orange II by ZnMn2O4 in a Novel Photo-Chemical Catalysis System. *Front. Chem. Sci. Eng.* 2020, 14, 956−966.

(16) WHO. *Guidelines for Drinking-Water Quality 1: Recommendations*, 3rd ed.; World Health Organization: Geneva, 2004.

(17) Barroso-Martín, I.; Moretti, E.; Talon, A.; Storaro, L.; Rodríguez-Castellón, E.; Infantes-Molina, A. Au and AuCu Nanoparticles Supported on SBA-15 Ordered Mesoporous Titania-Silica as Catalysts for Methylene Blue Photodegradation. *Materials* 2018, 11, 1−17.

(18) Stoyanova, M.; Christoskova, St.; Georgieva, M. Mixed Ni-Mn-Oxide Systems as Catalysts for Complete Oxidation: Part II. Kinetic Study of Liquid-Phase Oxidation of Phenol. *Appl. Catal., A* 2003, 249, 295−302.